The Astrophysical Journal, 827:98 (7pp), 2016 August 20 doi:10.3847/0004-637X/827/2/98

THE EFFECTS OF EXPERIMENTAL CONDITIONS ON THE REFRACTIVE INDEX AND DENSITY OF LOW-TEMPERATURE ICES: SOLID CARBON DIOXIDE

M. J. Loeffler[1], M. H. Moore[1,2], and P. A. Gerakines[1]
[1] Astrochemistry Laboratory, Code 691, NASA Goddard Space Flight Center, Greenbelt, MD 20771, USA
[2] University Space Research Association, Code 691, NASA Goddard Space Flight Center, Greenbelt, MD 20771, USA
Received 2016 April 27; revised 2016 June 5; accepted 2016 June 8; published 2016 August 11

ABSTRACT

We present the first study on the effects of the deposition technique on the measurements of the visible refractive index and the density of a low-temperature ice using solid carbon dioxide (CO_2) at 14–70 K as an example. While our measurements generally agree with previous studies that show a dependence of index and density on temperature below 50 K, we also find that the measured values depend on the method used to create each sample. Below 50 K, we find that the refractive index varied by as much as 4% and the density by as much as 16% at a single temperature depending on the deposition method. We also show that the Lorentz–Lorenz approximation is valid for solid CO_2 across the full 14–70 K temperature range, regardless of the deposition method used. Since the refractive index and density are important in calculations of optical constants and infrared (IR) band strengths of materials, our results suggest that the deposition method must be considered in cases where n_{vis} and ρ are not measured in the same experimental setup where the IR spectral measurements are made.

Key words: astrochemistry – planetary nebulae: general – methods: laboratory: molecular – methods: laboratory: solid state – radiative transfer – techniques: spectroscopic

1. INTRODUCTION

The presence of low-temperature condensed volatiles (hereafter, simply "ice") is well-documented for a variety of extraterrestrial environments (Boogert et al. 2015). Remote sensing techniques, such as infrared (IR) spectroscopy, are used to detect the characteristic features of ice species, and comparisons to relevant laboratory-based studies make up crucial parts of the interpretation of the observed spectra.

In the interstellar medium (ISM), ices are detected by way of their IR absorption features as measured when radiation is transmitted through dense molecular clouds. Typically, the band area of each absorption feature is used to quantify the abundance of each ice component, using a parameter known as the band strength (or *A* value). Band strengths are measured in the laboratory, and the accuracy of the results relies on knowing both the thickness and the density of the lab sample (e.g., Hollenberg & Dows 1961; d'Hendecourt & Allamandola 1986). See the review by Bouilloud et al. (2015) for a recent compilation of measured IR band strengths for ices relevant to the ISM.

The surfaces of icy planetary bodies are observed by reflectance spectroscopy, and the abundances of surface components are constrained by models of light scattering from icy grains of assumed size distributions and compositions (Verbiscer et al. 2006). In order to create such a model, the optical constants—the real and imaginary components of the refractive index—of each component are needed as input parameters. Like band strengths, optical constants are derived from laboratory spectra, through a method such as the Kramers–Krönig analysis (Hudgins et al. 1993; Baratta & Palumbo 1998; Moore et al. 2010), and require accurate measurements of a sample's thickness and visible refractive index (n_{vis}).

Our group is currently measuring the optical constants and band strengths of ice samples for use in analyzing the spectra of extraterrestrial ices (Hudson et al. 2014a, 2014b; Gerakines & Hudson 2015a, 2015b). In most cases, we have made new measurements of n_{vis} for ice samples used in our analyses, because no values exist in the literature for the same conditions of temperature and ice phase (amorphous or crystalline). Similarly, the density (ρ) of ices are often unknown at these temperatures and phases, and studies in the literature either simply assume ρ to be 1 g cm^{-3} (Hudgins et al. 1993), take ρ from the literature (Gerakines & Hudson 2015b), or estimate ρ using the Lorentz–Lorenz relation (Brunetto et al. 2008).

Knowing that n_{vis} and ρ cannot always be measured in the laboratory and often must be adopted from the results of experiments performed under slightly different conditions, we have investigated how strongly these two quantities depend on certain experimental parameters. We focus here on solid CO_2, because it has been identified as an important component of multiple objects in both the solar system (e.g., Clark et al. 2014) and interstellar medium (e.g., Boogert et al. 2015; de Graauw et al. 1996).

The disagreement in the literature for n_{vis} and ρ for solid CO_2 at cryogenic temperatures also motivated this study. For instance, reported values for n_{vis} near 70–80 K vary from 1.34 (Kruger & Ambs 1959) to 1.46 (Tempelmeyer & Mills 1968). Values in the 4–20 K range vary from 1.22 (Kruger & Ambs 1959; Satorre et al. 2008) to 1.27 (Wood & Roux 1980). Disagreements have also been noted in the reported values for ρ: near 80 K, published values range from 1.5 to 1.65 g cm^{-3} (Smedt & Keesom 1924; Maass & Barnes 1926), and at lower temperatures they range from 0.98 to 1.08 g cm^{-3} (Schulze & Abe 1980; Wood & Roux 1980; Satorre et al. 2008).

We point out that the dependence of n_{vis} and ρ on the deposition temperature observed for solid CO_2 has been attributed to the porosity of the sample, which decreases with increasing temperature, as indicated by gas adsorption measurements (Schulze & Abe 1980). As such, it is possible that the variation in n_{vis} and ρ may be the result of real structural differences in the prepared ice samples. Thus, to test the sensitivities of n_{vis} and ρ to different deposition conditions for the case of solid CO_2, we have made measurements between 14 and 70 K utilizing five different experimental

configurations. To our knowledge, this is the first study that directly tests the importance of the deposition conditions on n_{vis} and ρ. The data presented in the following sections can be used to improve the consistency and accuracy of n_{vis} and ρ measurements for low-temperature ices, yielding more accurate band strengths and optical constants for astronomically important ice components such as CO_2.

2. EXPERIMENTAL DETAILS

All experiments were performed inside a stainless-steel ultra-high vacuum chamber on a radiation-shielded cryostat (a schematic is shown in Figure 1). The base pressure of the chamber was ~0.5–1 × 10^{-10} Torr, and inside the radiation shield it is estimated to be 10–100 times lower. Solid carbon dioxide samples were vapor-deposited between 14 and 70 K with a flux of 8 × 10^{14} molecules cm^{-2} sec^{-1} (~1.5 μm hr^{-1}), using five different deposition configurations (as described in Table 1). The deposition techniques are described in more detail in Section 2.1.

Samples were condensed onto an optically flat, gold-mirror electrode of an Inficon IC6 quartz-crystal microbalance (QCM). The resonance frequency of the crystal was monitored using an Inficon IC6 controller to a resolution of better than 0.1 Hz. During growth, the intensities of two 670-nm laser beams reflected from the mirror were monitored with photodiodes connected to inverting operational amplifiers (current-to-voltage converters). The incidence angles of the lasers were measured to be 3.57 ± 0.04° and 53.56 ± 0.24°, respectively, where the uncertainties are due predominantly to the vacuum chamber manufacturer's design tolerances. The IR specular reflectance of each sample was measured at an incidence angle of 37.5° using a Thermo-Nicolet Nexus 6700 Fourier-transform IR spectrometer operating from 6000 to 650 cm^{-1} (1.67 to 15.4 μm) at a resolution of 1 cm^{-1}.

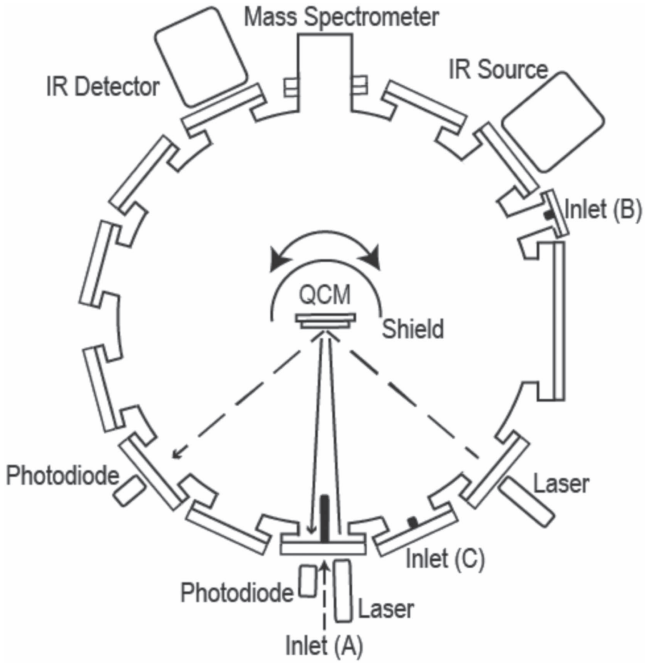

Figure 1. Schematic cross section of the experimental setup. The gas inlet (B) is 35° below the plane of the diagram; all other inlets and instruments shown are in the same plane. The diameter of the chamber is 14.00″.

The refractive index of our ice samples, n_{vis}, at 670 nm was calculated according to

$$n_{vis} = \sqrt{\frac{\sin^2\theta_2 - \left(\frac{t_1}{t_2}\right)^2 \sin^2\theta_1}{1 - \left(\frac{t_1}{t_2}\right)^2}}, \quad (1)$$

where θ_1 and θ_2 are the incidence angles of the lasers, and t_1 and t_2 are the periods of oscillation in their respective interference signals during deposition (Tempelmeyer & Mills 1968; Satorre et al. 2008; Romanescu et al. 2010). In general, the period of each oscillation can be calculated by recording the time of each minimum and maximum, plotting these values versus the fringe number and determining the slope. See Figure 2 for an example. We note that as the larger-angled laser showed relatively broader maxima, making the exact time of the peak more uncertain, we calculated the period using only the fringe minima.

The ice thickness, h (in nm), was determined from the laser interference measurements using the well-known formula from Heavens (1965),

$$h = \frac{N_f \lambda}{2\sqrt{n_{vis}^2 - \sin^2\theta}}, \quad (2)$$

where N_f is the number of interference fringes observed, λ is the laser wavelength (670 nm), and θ is the incidence angle of the laser. To obtain the most accurate measurement of h, we used the small-angled laser ($\theta = \theta_1$) because $\sin\theta_1 \ll n_{vis}$.

The QCM was used to measure ρ (in g cm^{-3}) by observing the change in the crystal's resonance frequency during ice

Table 1
Refractive Index (at 670 nm) and Density for Solid CO_2 for the Different Deposition Methods Used in This Study

Method	Inlet	Description	Diffuser in Place?	Thermal Shield in Place?	Distance from Inlet to Substrate (cm)	30 K		70 K	
						n_{vis}	ρ (g cm^{-3})	n_{vis}	ρ(g cm^{-3})
1	A	0° Incidence	Yes	Yes	13	1.34 ± 0.01	1.44 ± 0.01	1.40 ± 0.01	1.68 ± 0.01
2	A	0° Incidence	No	Yes	13	1.36 ± 0.01	1.56 ± 0.01	1.40 ± 0.01	1.70 ± 0.01
3	B	Background deposit	No	Yes	18	1.33 ± 0.01	1.40 ± 0.01	1.40 ± 0.01	1.68 ± 0.01
4	B	Background deposit	No	No	18	1.31 ± 0.01	1.33 ± 0.01	1.40 ± 0.01	1.67 ± 0.01
5	C	20° Incidence	No	Yes	18	1.35 ± 0.01	1.48 ± 0.01	1.42 ± 0.02	1.69 ± 0.02

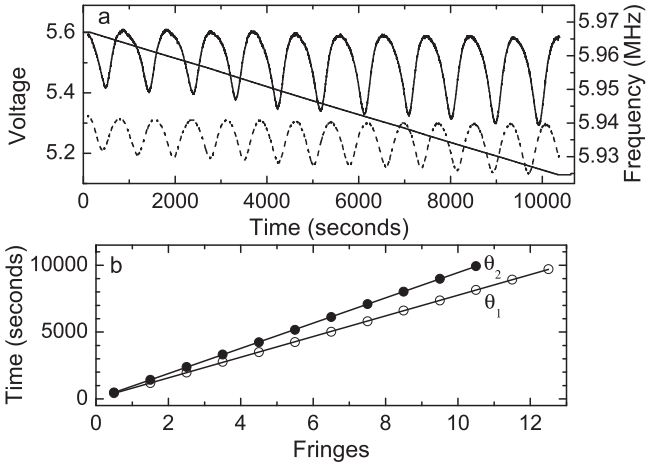

Figure 2. Panel (a): the reflected intensities of the small-angle (dashed line) and large-angle (solid line) lasers during the growth of a solid CO_2 sample at 60 K at 0° incidence angle (Method 1). The decrease in the frequency of the QCM during growth is also shown (black line, right axis). Panel (b): the times when the intensity traces (top, Figure 2(a)) have their minimum values are plotted vs. fringe number. The solid lines are linear fits to each set of data.

condensation and using the relation

$$\rho = \frac{\kappa}{h}\left(\frac{1}{f_1} - \frac{1}{f_0}\right), \tag{3}$$

where h is the sample thickness calculated using Equation (2), but converted into centimeter units, f_0 and f_1 are the initial and final frequencies of the crystal (in Hz), and κ is a constant, equal to 4.417×10^5 Hz g cm^{-2} (Lu & Lewis 1972).

2.1. Deposition Techniques

In this study, we chose to focus on deposition methods that may be typical, and most easily reproduced, in a given laboratory setup. To our knowledge, this is the first study that will allow one to determine the influence that a number of experimental variables have on the resulting n_{vis} and ρ for a low-temperature ice. A detailed summary of each method is given in Table 1. In Methods 1 and 2 (Inlet A), the deposition tube was positioned so that it pointed perpendicular to the substrate (i.e., at an incidence angle of 0°). In Method 1, we created a diffuser by inserting a screw into the end of the deposition tube, forcing the gas to flow through the tortuous volume between the screw threads and the tube inner wall, and in Method 2 the tube was unblocked. In Methods 3 and 4 (Inlet B), the deposition tube was positioned in a direction that allowed no direct flux to the substrate, essentially creating a sample that was background deposited. Method 4 differs from Method 3 only in that the radiation shield surrounding the sample was removed. In Method 5 (Inlet C), an unblocked deposition tube was aimed at the substrate with an incidence angle of 20°. In all cases, the inner diameter of deposition tube was ~4 mm.

2.2. Error Analysis

In order to make quantitative comparisons among our different sets of results and to compare them to data in the literature, we calculated the precision and accuracy of our values of n_{vis} and ρ using standard error propagation techniques. The precision was estimated in each case by making the same measurement several times under the same experimental conditions and taking the standard deviation of the results. The resulting deviation in n_{vis} and ρ was typically 0.001 and 0.003 g cm^{-3}, respectively. In a few cases the deviation was larger by about a factor of 10. The given error bars in n_{vis} and ρ reflect the corresponding precision estimates in each case.

The absolute uncertainties of our measurements are given by the uncertainties in the parameters used to calculate n_{vis} and ρ, resulting in an offset for all of our measurements, regardless of the precision. Given that n_{vis} is calculated from (1), the absolute uncertainty, $u(n_{vis})$, can be determined by differentiating (1) with respect to each variable and applying standard error propagation techniques, resulting in

$$u(n_{vis}) = \sqrt{\left[\frac{\partial n_{vis}}{\partial t_1}u(t_1)\right]^2 + \left[\frac{\partial n_{vis}}{\partial t_2}u(t_2)\right]^2 + \left[\frac{\partial n_{vis}}{\partial \theta_1}u(\theta_1)\right]^2 + \left[\frac{\partial n_{vis}}{\partial \theta_2}u(\theta_2)\right]^2}. \tag{4}$$

Similarly, combining Equations (2) and (3) and differentiating the result with respect to each dependent term yields Equation (5).

$$u(\rho) = \sqrt{\left[\frac{\partial \rho}{\partial n_{vis}}u(n_{vis})\right]^2 + \left[\frac{\partial \rho}{\partial N_f}u(N_f)\right]^2 + \left[\frac{\partial \rho}{\partial f_0}u(f_0)\right]^2 + \left[\frac{\partial \rho}{\partial f_1}u(f_1)\right]^2 + \left[\frac{\partial \rho}{\partial \theta_1}u(\theta_1)\right]^2}. \tag{5}$$

As an example, for the experiment shown in Figure 2, we measured $u(t_1) = 1.6$ s and $u(t_2) = 1.5$ s, leading to $u(n_{vis}) = 0.01$. We estimated $u(N_f) = 0.01$ and $u(f_0) = u(f_1) = 40$ Hz by evaluating $u(t)$ for a single interference minima. Combining these values with the uncertainties given above yields $u(\rho) = 0.01$ g cm^{-3}. These values are typical for all of the measurements reported here.

3. RESULTS

In Figure 3, our values of n_{vis} and ρ for solid CO_2 are plotted versus deposition temperature for the first four of the deposition methods described in Section 2.1. A distinct trend with temperature is apparent in all four cases: n_{vis} and ρ increase with T until ~50 K, and above 50 K there is no clear T dependence (n_{vis} and ρ are approximately constant). In addition, both n_{vis} and ρ depend on the deposition approach when $T < 50$ K. The similarity of the relationship of n_{vis} and ρ with temperature is discussed in Section 4.

As shown in Figure 3(a), the total change in n_{vis} over the entire temperature range for a single deposition method was ~0.12 (~10%). At a given temperature, the lowest values of n_{vis} were measured when the sample was background deposited (Methods 3 and 4). Of these, the configuration where the radiation shield was removed (Method 4) produced the lowest value for n_{vis} (Table 1). The highest values at each temperature were measured when the gas flowed through an unblocked deposition tube aimed at the substrate at an incidence angle of 0° (Method 2). The difference in n_{vis} between Methods 2 and 4 at the lowest attainable temperature for Method 4 (30 K) was ~0.05 (~4%).

In Figure 3(b), the total change in ρ over the entire temperature range for a single deposition method was ~0.4 g cm^{-3} (~30%). As with n_{vis}, the measured values of ρ for samples deposited below 50 K also varied with the deposition

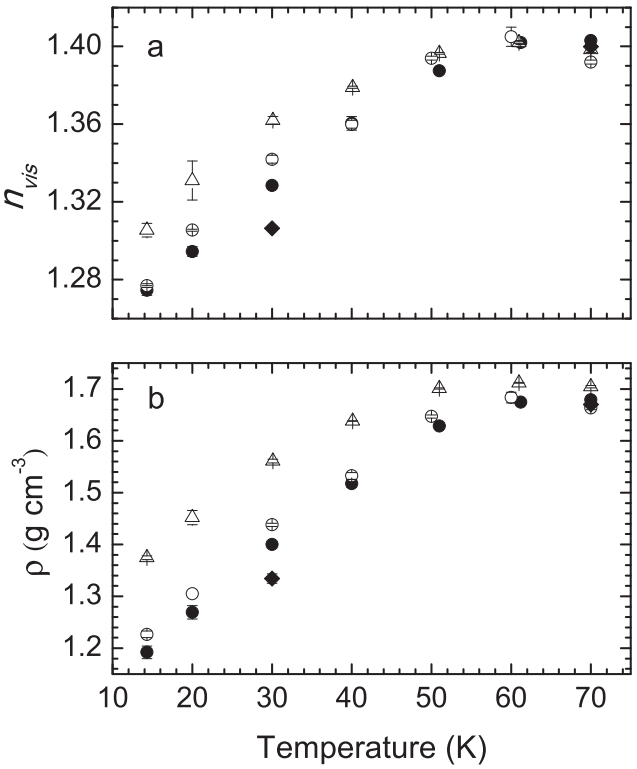

Figure 3. Index of refraction at 670 nm (a) and density (b) of solid CO_2 as a function of growth temperature. Symbols correspond to the following deposition methods 1 (Δ), 2 (o), 3 (•), and 4 (♦) described in Table 1. Error bars show the precision of the measurements.

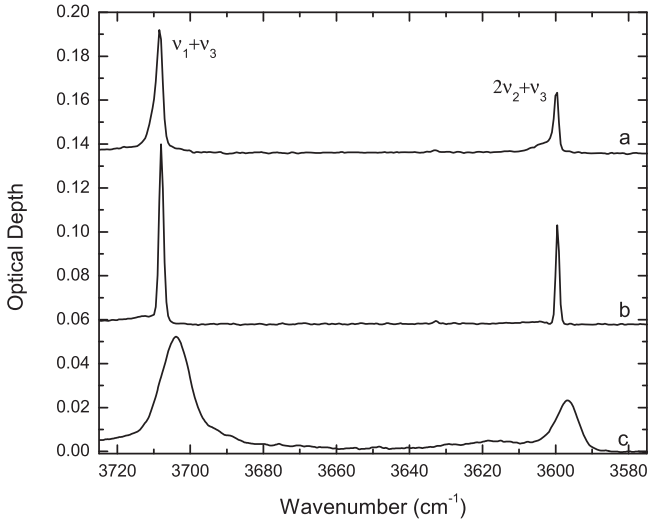

Figure 4. Infrared spectrum of solid CO_2 at 14 K after (a) depositing at 14 K and (b) depositing at 70 K and cooling to 14 K. Spectrum (c) is the transmission spectrum of solid amorphous CO_2 deposited at 10 K using the system described by Gerakines & Hudson (2015a). In each case, the thickness of the deposited sample was ∼0.1 μm.

method. Again, the lowest values of ρ were measured for the samples that were background deposited (Methods 3 and 4) with Method 4 producing the lowest value (Table 1), and the highest values were measured for the ones where the gas flowed through an unblocked deposition tube (Method 2). The difference in ρ between Methods 2 and 4 at 30 K was ∼0.23 g cm^{-3} (∼16%).

In addition to measuring n_{vis} and ρ, we also recorded the IR spectrum for each solid CO_2 sample, allowing us to evaluate each ice's phase (amorphous or crystalline). As an example, in Figures 4 (a)–(b), we show near-IR spectra from 3750 to 3550 cm^{-1} for two CO_2 ices deposited using Method 1. Also shown (Figure 4(c)) is the absorbance spectrum of an amorphous solid CO_2 sample measured at 10 K by Gerakines & Hudson (2015a). The sample corresponding to spectrum (a) in Figure 4 was grown at 14 K with no further processing. For (b), the sample was grown at 70 K, where it is crystalline, and cooled to 14 K before recording the IR spectrum. The $\nu_1 + \nu_3$ and $2\nu_2 + \nu_3$ vibrational combination modes of CO_2 are clearly visible at 3708 cm^{-1} and 3600 cm^{-1}, respectively. Surprisingly, the profile of the absorption features in (a) are not significantly different from (b), despite the fact that in (a) the sample was never heated above 14 K. This indicates that, even at the lowest temperatures implemented in our experiments, our CO_2 ices are not amorphous (Figure 4(c)) but predominantly crystalline. Samples grown using the other deposition methods had similar IR spectra to those shown for Method 1, so the observation of crystalline CO_2 in Figure 4(a) is not a consequence of our deposition method. Furthermore, decreasing or increasing the growth rate by a factor of 10 had no effect on (a), suggesting that significantly lower rates and/or temperatures would be needed to create amorphous CO_2, consistent with our previous studies (Gerakines & Hudson 2015a). We have also noted similar difficulties in obtaining amorphous ethylene (Hudson et al. 2014a), acetylene (Hudson et al. 2014b), and methane (Gerakines & Hudson 2015b) ices. Thus, all of our n_{vis} and ρ measurements represent those of crystalline CO_2, regardless of the temperature at which the samples were created, and we would be incorrect to assume that our samples deposited at 14 K were amorphous merely on the basis of the temperature. These results, which are the first ones where the phase of the ice is identified for the same sample used in the n_{vis} and ρ measurements, clearly demonstrate the importance of verifying the phase of ice samples when n_{vis} and ρ measurements are reported.

4. DISCUSSION

4.1. Comparison with Previous Studies

Measurements of n_{vis} and ρ for solid CO_2 date back 90 years (e.g., Maass & Barnes 1926; Kruger & Ambs 1959). Table 2 lists several such results, which are also plotted in Figure 5 alongside our measurements for Methods 3 and 4. The value we measured for n_{vis} at 70 K was typically 1.40 ± 0.01, where Method 5 resulted in slightly higher values of 1.42 ± 0.02. The value measured for ρ at 70 K varied with the deposition method between 1.67 and 1.70 g cm^{-3}. Our results for n_{vis} compare well with some of the listed measurements given in Table 2 and shown in Figure 5 (e.g., Seiber et al. 1971; Schulze & Abe 1980; Wood & Roux 1980), as do our results for ρ (e.g., Maass & Barnes 1926; Wood & Roux 1980). Of the other studies listed in Table 2 and shown in Figure 5, where agreement is less satisfactory, two of them measure n_{vis} using the same technique described in our work (Satorre et al. 2008; Tempelmeyer & Mills 1968) and thus merit comment. One of these studies (Tempelmeyer & Mills 1968) published n_{vis} values at multiple wavelengths in the visible region. Their values appear to be higher than previous measurements near 600 nm (e.g., Seiber et al. 1971; Schulze & Abe 1980; Wood & Roux 1980) but lower than values reported near 1000 nm (Yamada &

Table 2
Refractive Index and Density Measurements for Solid CO_2 at 4–20 K and 70–80 K

	4–20 K		70–80 K		Reference
λ (nm)	$n(\lambda)$	ρ (g cm^{-3})	$n(\lambda)$	ρ (g cm^{-3})	
546.1	1.22	…	1.34	…	Kruger & Ambs (1959)
589	…	…	1.43	1.67	Seiber et al. (1971)
600	…	…	1.46	…	Tempelmeyer & Mills (1968)
632.8	1.27	1.08	1.43	1.67	Wood & Roux (1980)
632.8	1.25	1.08	1.42	1.78	Schulze & Abe (1980)
632.8	1.25	…	…	…	Baratta & Palumbo (1998)
632.8	1.22	0.98	1.35	1.5	Satorre et al. (2008)
632.8	1.22	…	1.31	…	Isokoski et al. (2014)
670	1.27[a]	1.20[a]	1.40[b]	1.67[b]	this work
1000	…	…	1.41	1.67	Seiber et al. (1971)
1000	…	…	1.38	…	Tempelmeyer & Mills (1968)
1100	…	…	1.41	…	Yamada & Person (1964)
…	…	…	…	1.63	Smedt & Keesom (1924)
…	…	…	…	1.67[c]	Maass & Barnes (1926)

Notes.
[a] Deposition Method 3.
[b] Deposition Methods 3 and 4.
[c] Measurement on bulk ice crystals.

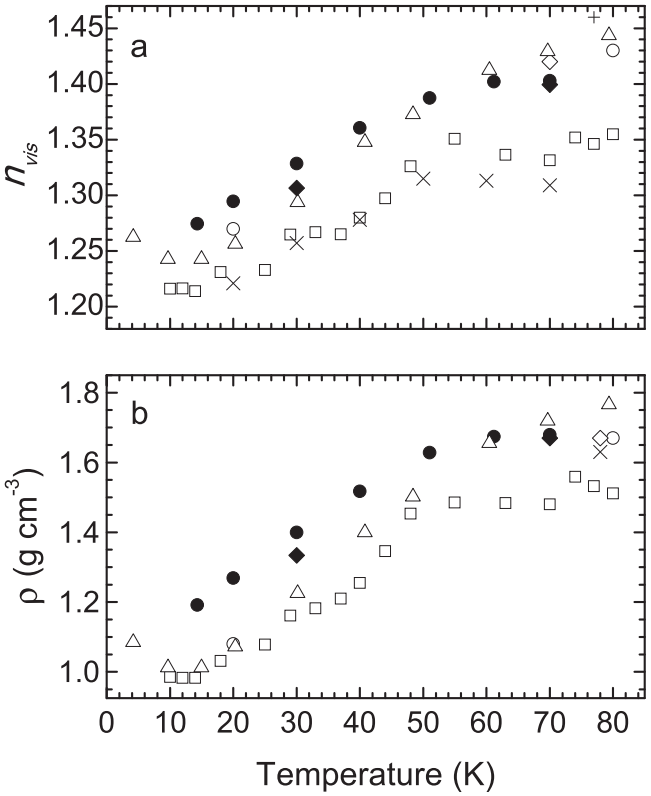

Figure 5. Refractive index and density of solid CO_2 plotted vs. deposition temperature compared with previous studies. Panel (a): this work; Method 3 (•) and Method 4 (♦), Schulze & Abe (1980) (Δ), Satorre et al. (2008) (□), Wood & Roux (1980) (o), Isokoski et al. (2014) (×), Tempelmeyer & Mills (1968) (+), Seiber et al. (1971) (◊). Panel (b): this work; Method 3 (•) and Method 4 (♦), Schulze & Abe (1980) (Δ), Satorre et al. (2008) (□), Wood & Roux (1980) (o), Smedt & Keesom (1924) (×), Maass & Barnes (1926) (◊). Refractive index values are only shown for measurements made between 600 and 700 nm.

Person 1964; Seiber et al. 1971). Seiber et al. (1971) suggested that the higher values obtained by Tempelmeyer and Mills at lower wavelengths were a consequence of the incident angle of the laser not being well-constrained ($\Delta\theta = 0.5°$) but did not give a reason for the discrepancy at longer wavelengths. Interestingly, the data obtained by Tempelmeyer and Mills near 700 nm nearly match the data of Seiber et al. (1971). Thus, it seems unlikely that the poor constraint of the laser incidence angle can explain the trend of these noted discrepancies because there is no systematic offset between the Seiber et al. and Tempelmeyer and Mills data sets. Although the data of Satorre et al. (2008) display a systematic offset from the other studies mentioned above (Table 2), it is unlikely that this same issue could also explain the differences in n_{vis} and ρ reported. The reported uncertainty in the laser incidence angle was only 0.2°, which, using our error propagation method, would only alter the refractive index by 0.005 and density by 0.0075 g cm^{-3}.

The study by Kruger & Ambs (1959) showed that n_{vis} of solid CO_2 changed with temperature, dropping by about 0.12 between 77 K and 4 K. Later measurements (see Table 2 and Figure 5) of n_{vis} and ρ for solid CO_2 supported the trend observed by Kruger & Ambs (1959), though most reported higher values for n_{vis}. To compare our results at low temperature ($T < 50$ K) to those of others, we focus on the studies that are also consistent with our high-temperature results. Of those studies, Schulze & Abe (1980) reported values near our lowest attainable temperature of 14 K. Depending on our deposition method, our n_{vis} values at 14 K ranged between 1.27 and 1.31 and ρ between 1.19 and 1.38 g cm^{-3}, which is 0.02–0.06 and 0.1–0.3 g cm^{-3} higher than that reported by Schulze & Abe (1980). Given that our results at 70 K are the same and also consistent with other studies, it is likely that the ices produced in our experimental setup are more compact than those measured by Schulze and Abe and this is likely a consequence of our experimental setup, in which the impinging gas will stick to the radiation shield unless it approaches the substrate in a limited range of incidence angles. We estimate that instead of a molecule being able to approach the substrate at a grazing angle (or near 90° with respect to the surface normal), our setup limits this such that a background deposited molecule would directly hit the substrate only if it approached the sample at an angle less than ~65° from the surface normal.

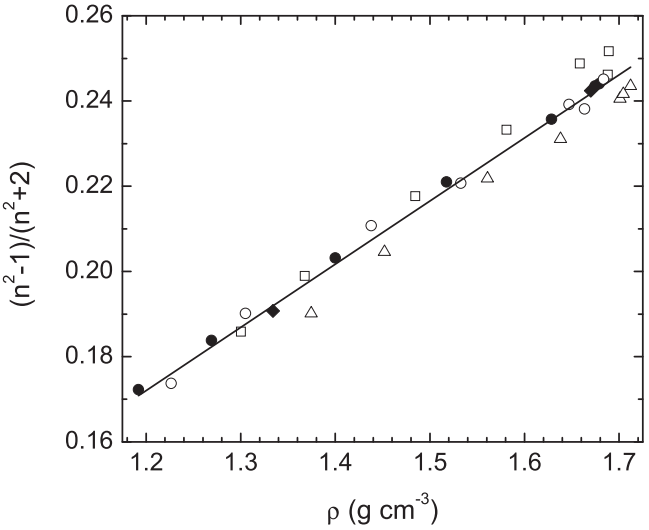

Figure 6. Using the refractive index and density values measured in this study (Figure 3), the left-hand side of the Lorentz–Lorenz approximation (Equation (6)) is plotted vs. density ρ. Plotting symbols correspond to the deposition method: 1 (Δ), 2 (○), 3 (•), 4 (♦), and 5 (□). A linear fit to the data, $y = 0.148\ x - 0.006$, is shown by the solid line, where the slope is the Lorentz–Lorenz coefficient L.

This hypothesis is supported by our finding that background depositing samples with the radiation shield removed from the system (Method 4) resulted in a decrease in $n_{\rm vis}$ by 0.03 and in ρ by 0.07 g cm^{-3} at 30 K, as compared to measurements made when the radiation shield was used (Method 3).

4.2. The Lorentz–Lorenz Approximation

The index of refraction n and density ρ of a given material are related by the Lorentz–Lorenz approximation (Lorentz 1880; Lorenz 1881). For materials that lack a dipole moment,

$$\frac{(n^2-1)}{(n^2+2)} = \frac{4\pi\alpha N_A}{3M}\rho, \qquad (6)$$

where α is the polarizability of the material (in cm^3 molecule^{-1}), M is its molar mass (in g mole^{-1}), and $N_{\rm A}$ is its Avogadro's number. If α is known, n can be estimated from measurements of ρ and vice versa.

Since α is roughly independent of temperature, a plot of the left-hand side of Equation (6) versus ρ for measurements made at several temperatures should resemble a line with a slope equal to the Lorentz–Lorenz coefficient, $L = (4\pi\alpha N_{\rm A})/(3M)$. Such a plot is shown in Figure 6, where we have used our measured values of $n_{\rm vis}$ and ρ for solid CO_2. The data are extremely well fit by a straight line, demonstrating the validity of the Lorentz–Lorenz approximation in this case regardless of the deposition method, which is in agreement with a recent study by Domingo et al. (2015) who utilized the data of Satorre et al. (2008). The best fitting line to our data yields a slope of 0.148 ± 0.006 cm^3 g^{-1}, with an r^2 statistic of 0.975. This is in reasonable agreement with the value of 0.155 cm^3 g^{-1} found by Wood & Roux (1980) for n measured at a wavelength of 632.8 nm. Furthermore, our L-value corresponds to an α of 2.58 ± 0.09 Å^3 molecule^{-1}, which is in good agreement with the value of 2.63 Å^3 molecule^{-1} reported for gas-phase CO_2 measured at 632.8 nm (Bridge & Buckingham 1966) and with the value of 2.48 Å^3 molecule^{-1} recently reported for solid CO_2 by Domingo et al. (2015) also measured at 632.8 nm.

Considering the measured uncertainty given in the fit to our data, using L as reported from our fit in Figure 6 for any deposition method we studied would, at worst, result in a density accurate to within 0.05 g cm^{-3} and a refractive index to within 0.015. However, we point out that we had the advantage of using multiple measurements to obtain L, which might not always be the case. If instead, as is often seen in the literature, we only used one data point to obtain L, our calculated ρ could be as much as 0.15 g cm^{-3} different than if we had used L obtained from our linear fit. Similarly, our calculated $n_{\rm vis}$ could be different by as much as 0.04.

4.3. Implications

To obtain the most accurate optical constants and absolute band strengths from the IR spectrum of a sample, ideally one should measure $n_{\rm vis}$ and ρ for that same sample. However, it is often not practical or even feasible to measure these values in the same experimental system used for IR transmission or reflectance spectroscopy. In those cases, our results for several deposition methods could be used, as described below, to estimate the error that may be introduced when these values are not measured directly.

For solid CO_2 deposited above 50 K, $n_{\rm vis}$ and ρ are relatively insensitive to growth conditions, and our measured values of 1.40 and 1.67 g cm^{-3}, could be applied, resulting in a relative error of only 1%–2%. Below 50 K, the uncertainties are larger because $n_{\rm vis}$ and ρ depend on both the temperature and the deposition method (see Figure 3 and Table 1). We have shown previously that varying $n_{\rm vis}$ by a few percent will induce a similar change in the optical constants n and k derived from IR transmission spectra (Hudson et al. 2014a). Thus, judging from our data and the results reported by Schulze & Abe (1980), for $T < 50$ K, the uncertainty in $n_{\rm vis}$ with respect to the experimental method would result in a relative error of only about 5% in calculated n and k values.

Band strengths (A values) depend on both $n_{\rm vis}$ and ρ and are therefore affected by a combination of their uncertainties. For instance, below 50 K, the absolute uncertainty in ρ can vary by as much as 0.30 g cm^{-3} at a single temperature, contributing to a relative error of up to 25% in the derived A-value.

The potential for error in derived A-values is high and could be reduced by a number of approaches. For instance, combining a measured value of $n_{\rm vis}$ and the value of L found here could reduce the relative error in a calculated A-value to less than 5%. We note that while the Lorentz–Lorenz approximation appears to be valid for solid CO_2, it is not clear whether this approach will also work for other condensed gases, but this could be tested. If measuring $n_{\rm vis}$ is not feasible, then the error in a derived A-value could still be reduced by simply choosing an experimental setup that mimics one of those described here. Of those listed, the easiest to reproduce, and most relevant to astrophysical ices, are Methods 3 and 4 (background deposition of gases). Alternatively, one could also use a diffuser (Method 1) to produce an ice that is similar to the background deposited ones. This would reduce the relative error in the derived values by about a factor of two, but probably not more than that, as other factors such as the

geometry of the radiation shield and proximity of the gas inlet to the sample may be more difficult to replicate.

5. CONCLUSIONS

In this study, we have performed the first investigation of the sensitivity of n_{vis} and ρ to the deposition method, using solid CO_2 as an example. In agreement with previous studies, we found that both parameters depend on temperature. In addition, we find that while the measured values of n_{vis} and ρ for solid CO_2 deposited above 50 K did not vary significantly with the deposition method, the measured values for ices deposited below 50 K do. In fact, at a single temperature, but with different deposition methods, n_{vis} varied by ~0.06 (~5%) and ρ varied by ~0.25 g cm^{-3} (~20%). We estimate that the variations observed in n_{vis} with this method could affect calculated optical constants of solid CO_2 by only about 5%. However, the density variations due to differences in experimental methods—observed in our work and other studies—suggest that the relative error in an assumed A-value could be as much as 25% if ρ is taken from the literature and not measured in the same system as the IR spectra. If one measures one of these parameters (either n_{vis} or ρ) and applies the Lorentz–Lorenz approximation, shown here to be valid for solid CO_2, then the relative error in A could be reduced to less than 5%. If measuring neither n_{vis} nor ρ is feasible, then the relative error in a derived A-value could be reduced by simply choosing a deposition method that mimics one of those described here and using our measured values.

The construction of the ultra-high vacuum chamber used in this study was partially supported by NASA Goddard's Technical Equipment fund. This work was supported by NASA's Astrophysics Research and Analysis (APRA) program. The authors thank Reggie Hudson for assistance in day-to-day operations in the laboratory and for his comments on this manuscript.

REFERENCES

Baratta, G., & Palumbo, M. 1998, JOSAA, 15, 3076
Boogert, A. C. A., Gerakines, P. A., & Whittet, D. C. B. 2015, ARA&A, 53, 541
Bouilloud, M., Fray, N., Bénilan, Y., et al. 2015, MNRAS, 451, 2145
Bridge, N. J., & Buckingham, A. D. 1966, RSPSA, 295, 334
Brunetto, R., Caniglia, G., Baratta, G. A., & Palumbo, M. E. 2008, ApJ, 686, 1480
Clark, R. N., Swayze, R. A., Carlson, R., Grundy, W., & Noll, K. 2014, RMGeo, 78, 399
de Graauw, T., Whittet, D. C. B., Gerakines, P. A., et al. 1996, A&A, 315, L345
d'Hendecourt, L. B., & Allamandola, L. J. 1986, A&AS, 64, 453
Domingo, M., Luna, R., Satorre, M. A., Santonja, C., & Millan, C. 2015, JLTP, 181, 1
Gerakines, P. A., & Hudson, R. L. 2015a, ApJL, 808, L40
Gerakines, P. A., & Hudson, R. L. 2015b, ApJL, 805, L20
Heavens, O. S. 1965, Optical Properties of Thin Solid Films (New York: Dover)
Hollenberg, J. L., & Dows, D. A. 1961, JChPh, 34, 1060
Hudgins, D. M., Sandford, S. A., Allamandola, L. J., & Tielens, A. G. G. M. 1993, ApJS, 86, 713
Hudson, R. L., Ferrante, R. F., & Moore, M. H. 2014a, Icar, 228, 276
Hudson, R. L., Gerakines, P. A., & Moore, M. H. 2014b, Icar, 243, 148
Isokoski, K., Bossa, J.-B., Triemstra, T., & Linnartz, H. 2014, PCCP, 16, 3456
Kruger, J., & Ambs, W. J. 1959, JOSA, 49, 1195
Lorentz, H. A. 1880, Wiedem Ann, 9, 641
Lorenz, L. 1881, Wiedem Ann, 11, 70
Lu, C. S., & Lewis, O. 1972, JAP, 43, 4385
Maass, O., & Barnes, W. H. 1926, RSPSA, 111, 224
Moore, M. H., Ferrante, R. F., Moore, W. J., & Hudson, R. 2010, ApJS, 191, 96
Romanescu, C., Marschall, J., Kim, D., Khatiwada, A., & Kalogerakis, K. S. 2010, Icar, 205, 695
Satorre, M. A., Domingo, M., Millan, C., et al. 2008, P&SS, 56, 1748
Schulze, W., & Abe, H. 1980, CP, 52, 381
Seiber, B. A., Smith, A. M., Wood, B. E., & Muller, P. R. 1971, ApOpt, 9, 2086
Smedt, J. d., & Keesom, W. H. 1924, Proc Amsterdam Acad, 27, 839
Tempelmeyer, K. E., & Mills, D. W. 1968, JAP, 39, 2968
Verbiscer, A. J., Peterson, D. E., Skrutskie, M. F., et al. 2006, Icar, 182, 211
Wood, B. E., & Roux, J. A. 1980, JOSA, 72, 720
Yamada, H., & Person, W. B. 1964, JChPh, 41, 2478